Interaction between Liénard and Ikeda dynamics in a nonlinear electro-optical oscillator with delayed bandpass feedback

Bicky A. Marquez,* Laurent Larger, Daniel Brunner, Yanne K. Chembo, and Maxime Jacquot
FEMTO-ST Institute, CNRS & University Bourgogne Franche-Comté, 15B Avenue des Montboucons, 25030 Besançon Cedex, France
(Received 6 September 2016; published 14 December 2016)

We report on experimental and theoretical analysis of the complex dynamics generated by a nonlinear time-delayed electro-optic bandpass oscillator. We investigate the interaction between the slow- and fast-scale dynamics of autonomous oscillations in the breather regime. We analyze in detail the coupling between the fast-scale behavior associated to a characteristic low-pass Ikeda behavior and the slow-scale dynamics associated to a Liénard limit-cycle. Finally, we show that when projected onto a two-dimensional phase space, the attractors corresponding to periodic and chaotic breathers display a spiral-like pattern, which strongly depends on the shape of the nonlinear function.

DOI: 10.1103/PhysRevE.94.062208

I. INTRODUCTION

Uncovering patterns in highly complex dynamical systems has always been a major challenge for the scientific community. Since the discovery of the Lorenz attractor [1] in 1963, the interest in understanding and exploring nonlinear dynamics increased continuously. The exploration of deterministic dynamics of nonlinear systems remains an active research topic today. Among the many models experiencing such complex behavior, nonlinear difference and differential equations have been useful for the description of many different real world phenomena, including steel beam motion between two magnets [2], chemical oscillators exhibiting chaotic behavior [3], or physiological control systems designed through the insertion of a time delay element [4].

Systems with delayed feedback display a broad variety of phenomena that are rarely observable in simpler systems governed by ordinary differential equations. Delay differential equations (DDEs) have been used for many applications, such as hyperchaotic signal generation [5–8]. A particular DDE that has inspired fundamental research as well as technological applications is the Ikeda equation [9,10], which describes the dynamics of a laser driven passive nonlinear ring resonator. Experimental realizations of DDEs implemented in an electro-optic (EO) system [11–14] allowed the development of high-performance broadband chaotic communications [15,16], ultrastable microwave sources [17–19], and random number generation [20]. The fundamental properties of networks of such oscillators has also received significant attention [21–24]. Another important application of DDEs also emerged recently as a branch of computer sciences. Using the Ikeda equation as an integral component of neuromorphic processors, it is possible to perform information processing and computing tasks [25–27]. In our current work an integral term is added to the original Ikeda equation, resulting in a band-pass effect due to this low frequency cutoff. As a consequence, the system is capable to show complex multiple time-scale dynamics.

The multiple time-scale behavior of the modified Ikeda system has been investigated using several approaches like stability and bifurcation analysis [13,28–31]. More recently, it was shown that such hybrid dynamics can be understood through the paradigm of Liénard systems with attractive-repulsive branches [32]. However, the description of the waveform evolution requires a more extensive analysis of the structural properties of the entire system.

It has been demonstrated that the structural shape of the phase space depends largely on the nonlinear function's characteristics. In fact, some well-established chaotic systems like Logistic, Tent and Bernoulli maps, Chua's circuit [33], Duffing-Holmes attractor [2], and the Ikeda equation are based on different kinds of nonlinear functions. Their contribution in the generation of complex and chaotic dynamics can be qualitatively described through the stretching and folding mechanism [34]. Stretching and folding results in exponential divergence of close orbits in certain phase-space regions. Trying to identify the relationship between nonlinear functions and their resulting dynamics, some reports show how complexity can be controlled by the nonlinear function extrema [35–37].

In this article, we propose a framework to characterize a delayed-feedback nonlinear optoelectronic oscillator based on the analysis of its nonlinear function. We analytically explain the integral term's impact for the modified Ikeda system. In particular, we characterize the route to spiral-like chaotic patterns in phase space, in dependency of feedback strength and operating point. The paper is organized as follows. In Sec. II we describe the nonlinear time-delayed EO oscillator and present the dimensionless coupled first-order delay differential equation. Section III contains a fixed point stability analysis in dependence of the operational point distance to the nonlinear function extrema. We confirm the validity of the model with experimental data. In Sec. IV, we analyze the Ikeda-Liénard dynamics of the system and perform an attractor reconstruction from the experimental time series. The last section concludes the article.

II. ELECTRO-OPTIC OSCILLATOR SETUP AND MODEL

The EO oscillator typically used for implementing an Ikeda system is illustrated in Fig. 1(a). It consists of the following devices: (i) A 1.55-μm semiconductor telecom laser diode whose optical power can be tuned from 0 to 20 mW. (ii) A Mach-Zehnder modulator (MZM) connected to the laser by an

*bicky.marquez@femto-st.fr

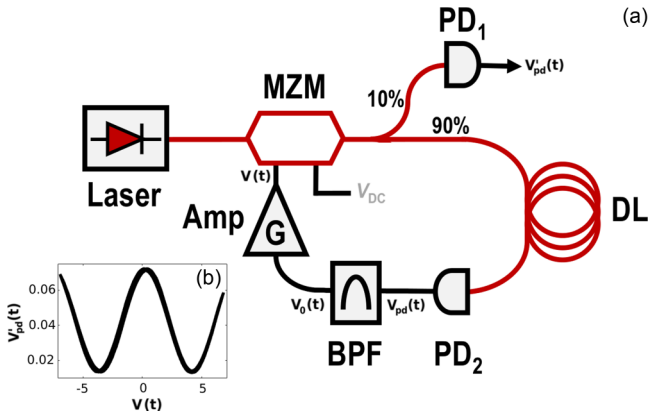

FIG. 1. (a) Schematic diagram of the nonlinear time-delayed EO setup. MZM, Mach-Zehnder modulator; PD, photodiode; DL, delay line; BPF, bandpass filter; Amp, RF amplifier. (b) Experimental record of the nonlinear transmission function showing an up to quartic-like approximated polynomial, with up to three accessible extrema.

optical fiber. The MZM performs the nonlinear transformation through its modulation transfer function,

$$P_{\text{out}}(t) = P_{\text{in}} \cos^2\left[\frac{\pi}{2}\frac{V(t)}{V_{\pi RF}} + \frac{\pi}{2}\frac{V_{DC}}{V_{\pi DC}}\right], \tag{1}$$

where the $V_{\pi DC} = 6.64$ V and $V_{\pi RF} = 3.80$ V are the DC and RF half-wave voltages of the modulator, respectively. The voltage $V(t)$ is the modulating signal while V_{DC} is the bias voltage that controls the operating point of the modulator. (iii) A 4-km-long optical fiber delay line, resulting in a delay time of $\tau_D \simeq 19.472\ \mu$s. (iv) An amplified photodiode detecting the light, and providing a voltage proportional to the optical intensity according to $V_{\text{pd}}(t) = SP_0(t - \tau_D)$, where $S = 1.08$ V/mW is the sensitivity of the InGaAS photodiode equipped with a transimpedance amplifier. (v) A bandpass filter with cutoff frequencies $f_{\text{l}} = 22.5$ Hz and $f_{\text{h}} = 0.6$ MHz. (vi) A radio-frequency amplifier with gain $G = 3.3$. The amplified signal is connected to the RF electrode of the MZM, thereby closing the feedback loop.

Assuming that the bandpass filter results from the cascade of first-order low-pass and high-pass filters with $f_{\text{l}} \ll f_{\text{h}}$, it can be shown that system dynamics can be described by a normalized integrodifferential delay equation, which is explicitly written as

$$x(t) + \tau\frac{dx}{dt}(t) + \frac{1}{\theta}\int_{t_0}^{t} x(\xi)\,d\xi = \beta\cos^2[x(t-\tau_D) + \phi_0], \tag{2}$$

where

$$x(t) = \frac{\pi V(t)}{2V_{\pi RF}}; \quad \phi_0 = \frac{\pi}{2}\frac{V_{DC}}{V_{\pi DC}}; \quad \beta = \frac{\pi G S P_{\text{in}}}{2V_{\pi RF}}; \tag{3}$$

$$\tau = \frac{1}{2\pi f_{\text{h}}}; \quad \theta = \frac{1}{2\pi f_{\text{l}}}. \tag{4}$$

For the dynamical system, the main control parameter β can be tuned through the laser power P_{in}. Furthermore, ϕ_0 stands for the bias offset phase of the MZM. Both β and ϕ_0 are bifurcation parameters for the oscillator. τ and θ are the characteristics fast and slow response times of the filter.

For mathematical purposes, it is convenient to rewrite Eq. (2) as a set of two-dimensionless coupled first-order DDEs with respect to the dimensionless time $\zeta = t/\tau_D$, resulting in

$$\begin{aligned} \varepsilon\,\dot{x}(\zeta) &= -x(\zeta) - \delta\,y(\zeta) + \beta\cos^2[x(\zeta-1) + \phi_0], \\ \dot{y}(\zeta) &= x(\zeta), \end{aligned} \tag{5}$$

with $\varepsilon = \tau/\tau_D$ and $\delta = \tau_D/\theta$.

III. DYNAMICS OF THE AUTONOMOUS SYSTEM

In the following, the dynamical characteristics of the time-delayed EO oscillator are briefly analyzed. A first step is the stability analysis of the trivial fixed point, which can be investigated by deriving an eigenvalue characteristic equation obtained after assuming perturbations proportional to $e^{\lambda\zeta}$ in Eq. (5):

$$\lambda^2 + \lambda[1 + \beta\sin(2\phi_0)e^{-\lambda}] + \varepsilon = 0. \tag{6}$$

The analysis of this transcendental equation reveals that the trivial fixed point is stable when $|\beta\sin(2\phi_0)| < 1$; beyond this limit, a Hopf-bifurcation might arise. In this case, the solution of Eq. (6) becomes purely imaginary ($\lambda = i\omega$), and we obtain the following equations:

$$\begin{aligned} \omega\tan\omega &= \delta - \varepsilon\omega^2, \\ -\beta\sin(2\phi_0) &= (\cos\omega)^{-1}. \end{aligned} \tag{7}$$

The first equation of Eqs. (7) defines the eigenmodes of the system, allowing us to analytically calculate the Hopf angular frequency. The second equation describes the section of the nonlinear function where the oscillation is possible, as a function of each angular frequency. For sections of the nonlinear function with a positive slope, we find that the eigen angular frequency is $\omega \simeq \sqrt{\delta}$, corresponding to a slow oscillation. Figures 2(a)–2(c) show corresponding slow oscillations. For operation along the negative slope we obtain $\omega \simeq \pi$, hence the period of oscillation is approximately twice the delay time.

When $-\beta\sin(2\phi_0) > 1$, a mixed-mode oscillation appears [32]; see Figs. 2(d)–2(f). It results from the superposition of two waveforms: (i) a slow-scale periodic signal, with 5-ms period, which is consistent in magnitude with the value obtained at the Hopf threshold for the slow eigenfrequency, $\omega = \sqrt{\delta}$, leading to a physical period of $2\pi\tau_D/\omega = \sqrt{2\pi\tau_D/f_{\text{l}}} \simeq 2.3$ ms. There, the curves at the top and bottom of the time series correspond to relaxation oscillations separated by sudden jumps. (ii) The fast-scale dynamics generated in the extrema's neighborhood of the periodic time series. Finally, dynamics with a strong coexistence of both time scales are shown in Figs. 2(g)–2(i). Through a qualitative inspection of the nonlinear function in Figs. 2(a), 2(d), and 2(g), one can observe that the sections of the nonlinear function with a negative slope increase with β. This causes the emergence of fast-scale oscillations with period $T = 40\,\mu s = 2\tau_D$ at the extrema of the slow envelop; see Figs. 2(e), 2(f), 2(h), and 2(i). Here, the decay in the temporal envelopes for the fast-scale oscillations are related to the existence of relaxation epochs. Such epochs

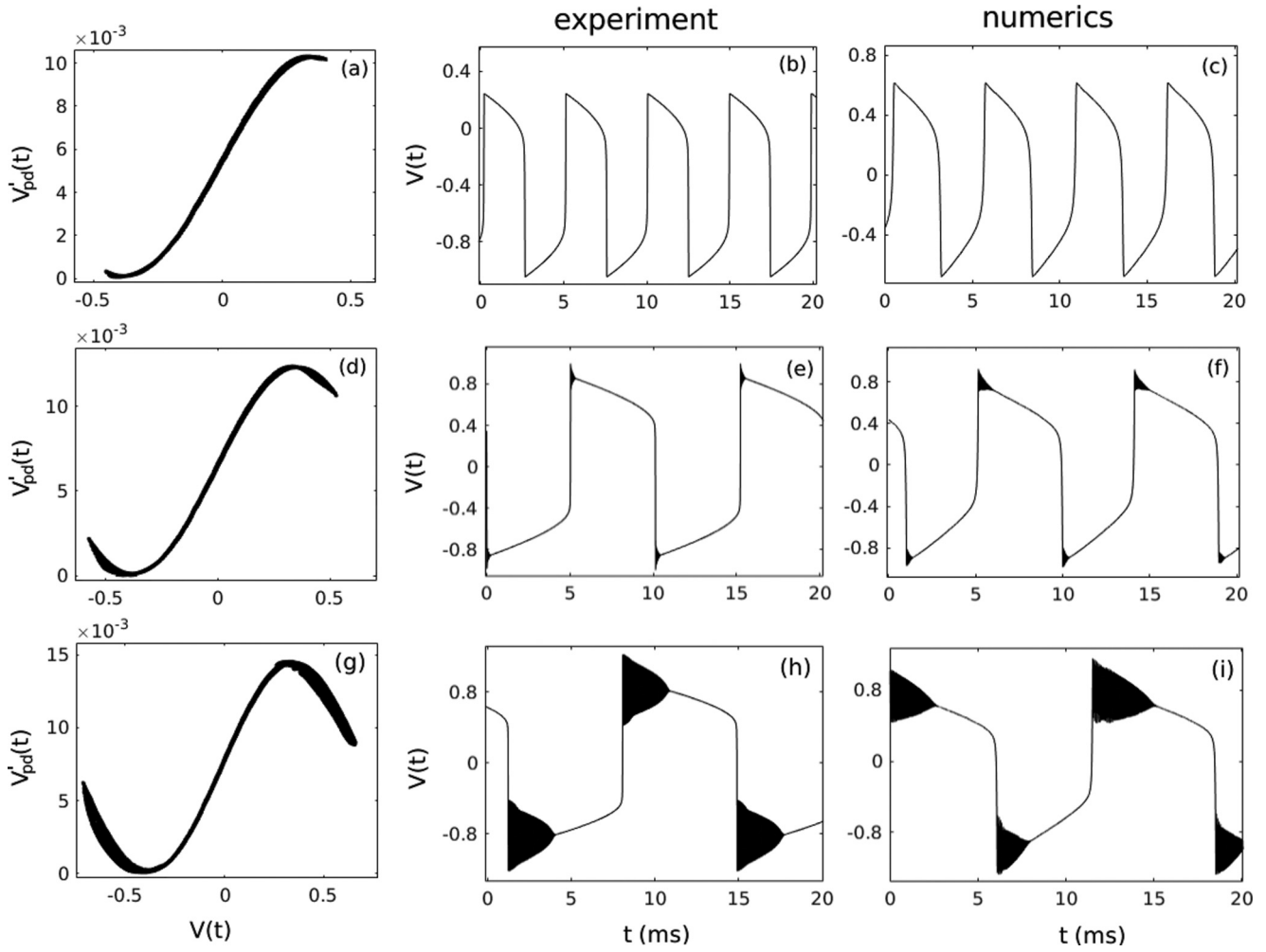

FIG. 2. Experimental and numerical results normalized gain β set to 1.4 (first row), 1.7 (second row), and 2.2 (third row). Left column: Transmission function of the MZM when operated at the middle inflection point with positive slope ($\phi_0 = -\pi/4$). Central column, experimental time traces; right column, numerical time traces.

are fast-time-scale oscillations occurring in the neighborhood of the nonlinear function extrema and along its negative slopes. This highlights the importance of the nonlinear function's shape in the actual dynamical solution. In addition, one can see that the period of the slow envelope continuously increases with growing β, from 2.3 ms at the slow envelope Hopf threshold ($\beta \simeq 1$), to 14 ms in Figs. 2(g)–2(i), through 5 ms in Figs. 2(a)–2(c) and 10 ms in Figs. 2(d)–2(f). Such a period of growth is consistent with the analytical study reported in Ref. [31].

By zooming in the extrema's neighborhood of the time series when $\{\beta = 2.2, \phi_0 = -\pi/4\}$, it can be seen that fast-scale oscillations have an obvious correspondence with the dynamics generated by the isolated parts of the nonlinear function with negative slope, where $\{\beta = 2.2, \phi_0 = -\pi/2; 0\}$. Figures 3 and 4 show time series for $\phi_0 = -\pi/4$ and $\phi_0 = -\pi/2; 0$, respectively. In Figs. 3(b) and 3(c) focus on the top and bottom of the nonlinear function. In Fig. 4, these two extrema are disconnected, with dynamics shown in panels (c) and (d). Under both conditions, dynamics are qualitatively comparable, having the same oscillation period $T \simeq 2\tau_D \simeq 40\ \mu$s as predicted by Eqs. (7) for the first fast eigenmode, with a very similar theoretical value compared to standard Ikeda model with double delay periodicity.

IV. THE LIÉNARD-IKEDA APPROACH

In this section, we analyze the interaction between the two time scales involved in the regime of breather oscillations. We therefore focus on the configuration where $\phi_0 = -\pi/4$, resulting in perfectly symmetric oscillations. One should notice that the particular case $\Phi_0 = -\pi/4$ is used here for analytical convenience only, resulting in the perfect symmetry conditions assumed in the original Liénard limit cycle theorem. Deviations away from $-\pi/4$, however, do not modify qualitatively the observed waveform, essentially changing the duty cycle of the slow motion. This was already underlined in previous references such as Ref. [32]. In the particular case of $\Phi_0 = -\pi/4$, Eq. (5) can be rewritten as

$$\ddot{x} + \dot{x} - \beta \cos[2x(\zeta - 1)]\dot{x}(\zeta - 1) + \varepsilon x = 0. \qquad (8)$$

In order to recover the textbook equation for Liénard system [38] from the previous equation of a bandpass EO delay dynamics, one needs to apply a new change of variable

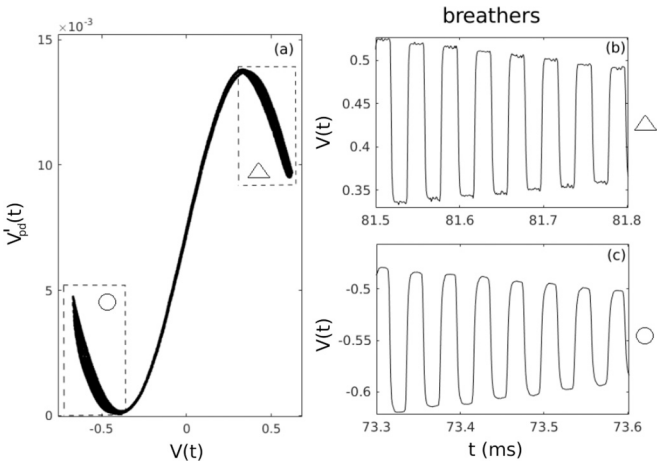

FIG. 3. (a) MZM transmission function with labels {△,◯} for the portions with negative slope. Zoom at the top (b) and bottom (c) of the time series showing mixed-mode dynamics, where $\beta = 2.2$ and $\phi_0 \simeq -\pi/4$. Both with period $T = 40\,\mu s = 2\tau_D$.

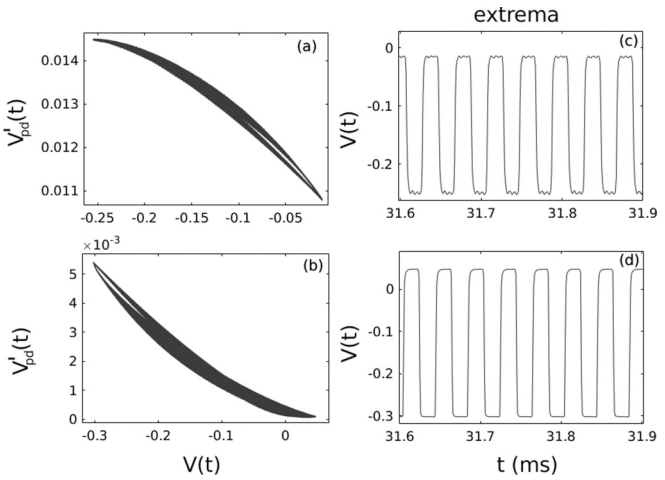

FIG. 4. MZM transmission functions for $\beta = 2.2$, if $\phi_0 \simeq 0$ (a) and $\phi_0 \simeq -\pi/2$ (b). Time series associated to the nonlinear function with $\phi_0 \simeq 0$ (c) and $\phi_0 \simeq -\pi/2$ (d). Both with period $T = 40\,\mu s = 2\tau_D$.

$s = \zeta\sqrt{\delta/\varepsilon}$. Doing this and assuming that the delay can be neglected compared to the time scales of the Liénard cycle, one indeed obtains

$$\ddot{x} + F'(x)\dot{x} + G'(x) = 0, \tag{9}$$

where

$$F'(x) = \frac{1}{\sqrt{\varepsilon\delta}}\left[1 - \beta\cos(2x)\right] \tag{10}$$

is an even function scaling the nonlinear damping, while $G'(x) = x$ is an odd function corresponding to the restoring force. This associated function $F(x)$ is determined from $F'(x)$ in Eq. (10). The Liénard plane is thus defined as

$$\dot{x} = y - F(x), \tag{11}$$

$$\dot{y} = -g(x), \tag{12}$$

where

$$F(x) = \int_0^x F'(\xi)\,d\xi = \frac{1}{\sqrt{\varepsilon\delta}}\left[x - \frac{1}{2}\beta\sin(2x)\right], \tag{13}$$

and $g(x) = G'(x)$ are smooth odd functions. From here it is possible to obtain the Liénard xy plane, which provides the exact solutions for the nonlinear transformations shown in Figs. 2(a), 2(d), and 2(g). According to the theorem ruling Liénard equation and its possible limit cycle solutions, Eqs. (11)–(13) have stable limit cycles if $F(x)$ has exactly three zeros with $F'(0) = (\varepsilon\delta)^{-\frac{1}{2}}[1-\beta] < 0$ if $\beta > 1$, and $F(x) \to \infty$ if $x \to \infty$ [38]. A more detailed analysis of the Liénard derivation and bandpass Ikeda dynamics, as well as its detailed discussion in the xy plane, can be found in Ref. [32].

The previous transformation of the bandpass EO delay dynamics into a Liénard system is helpful to discuss our main finding concerning the regime depicted in Figs. 2 to 6. In the EO bandpass delay system with moderate feedback ($\beta = 1$ to ca. 3), fast and slow timescales are in fact nonlinearly coupled, however, in an unidirectional way. Fast dynamics obey the standard Ikeda equation, while slow dynamics follow a Liénard limit cycle. The slow Liénard cycle actually drives the operating point Φ_0, around which a fast conventional Ikeda dynamics (i.e., low pass model, without the integral term) develops. To demonstrate this physically, we have performed a simple experiment in which the Liénard compound is replaced by an external triangular waveform modulating the offset phase parameter. The triangular shape of the waveform is motivated by the fact that the external drive is intended to replace the integral variable y of the original bandpass delay dynamics. This variable is indeed the long-time-scale integral of the variable x, which can be approximated, on average (due to the slow integration time of concern), by a constant, whether positive or negative. The corresponding integral is then simply a triangular waveform. Such a system is then modeled by

$$\varepsilon\frac{dz}{dt}(t) = -z(t) + \beta\cos^2[z(t) + \Phi_0 + u(t)], \tag{14}$$

where $u(t)$ is a triangular waveform having an amplitude and a period tuned, so that its effects emulate the actually observed slow oscillation of the Liénard limit cycle. One could notice that the previous Eq. (14) can be obtained from the bandpass Ikeda model in Eq. (5), setting $z(t) = x(t) + \delta y(t)$ and $u(t) = -\delta y(t)$, and assuming that the term $\varepsilon\delta\dot{y}$ is a negligible derivative in time compared to $\varepsilon\dot{z}$, due to the smallness of δ. Experimental and numerical results are shown in Fig. 5, where both the global shape as well as finer details at fast time scales are in excellent agreement. Experimentally, the forcing $u(t)$ of the standard Ikeda system was implemented by modulating ϕ_0 through the MZM's DC input, with amplitude $V_{DC} = 5.9\,\mathrm{V}$ and frequency 211 Hz. By using these values we approximate the slow periodic envelope of the bandpass Ikeda with the triangular signal, whose frequency is typically around 200 Hz. Furthermore, the amplitude of the triangular signal spans the full extrema neighborhood of the nonlinear function, $\phi_0 \in \{-\pi/2, \ldots, 0\}$, where the Ikeda-like dynamics are dominant. The time traces exhibit Ikeda-like oscillations combined with periodic breathing at the frequency of the external modulation. Consequently, it can be deduced that the evolution of the system displays Ikeda-like oscillations close

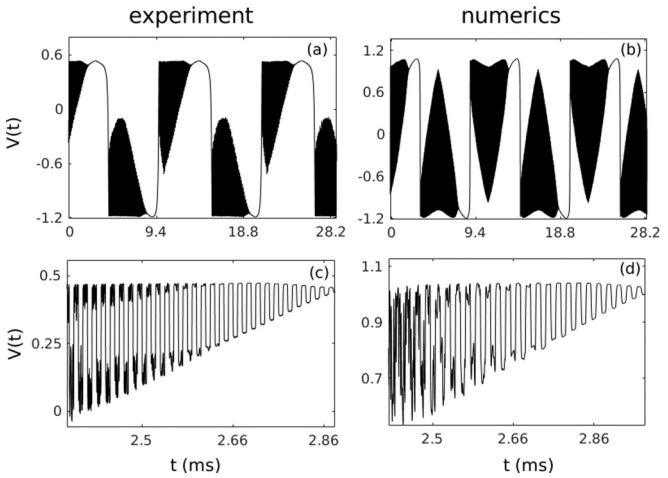

FIG. 5. (a, b) Breathers-like dynamics can be generated by changing periodically the MZM operating point in the Ikeda EO setup, and (c, d) zoom at the top of the time series.

to the extrema neighborhood, while the integral part induces slow-time-scale Liénard-like oscillations.

It is informative to illustrate the system's dynamics in a two-dimensional (2D) phase space using an attractor reconstruction technique. This procedure is carried out by using an additional time-delay coordinate $x(\zeta - 1)$, which allows us to project the original attractor onto a two-dimensional phase space. In order to implement this method, we have recorded an experimental time trace from the EO experimental setup, and used it to obtain the coordinates for the time-delay-based 2D-embedding. Figure 6 shows two-dimensional projections of the reconstructed attractors in the phase space for two types of breathers, where $\beta \in \{1.7, 2.2\}$. The existence of a large limit cycle is revealed by the slow-scale dynamics corresponding to the Liénard dynamics. The spiral-like trajectories in the limit cycle represent the fast-scale Ikeda-like solutions in the 2D-projection. This behavior is maintained even when the fast-scale dynamics has a chaotic nature. The spiral-shaped pattern of the attractor is related to the relaxation dynamics of the system induced by the slow-scale periodic oscillation, which yields a decaying in time envelope for the Ikeda-like waveforms. This spiral pattern is therefore the topological signature of a global interaction of two different dynamics, which are interacting nonlinearly with different time scales, however, unidirectionally from the slow motion (θ) into the fast ones (τ_D and τ).

V. CONCLUSION

We have investigated the dynamics of a bandpass delayed nonlinear EO system, and their particular slow-fast solutions, when the nonlinear feedback involves a positive slope between two extrema. Depending on the strength of the nonlinear delayed feedback weighted by the bifurcation parameter β, various solutions are bifurcating. Figure 7 illustrates such a sequence of bifurcations, from the Hopf point to highly complex fully developed chaos, as parameter β is increased from zero. The particular parameter conditions of concern have been recently investigated in the view of Liénard limit cycle.

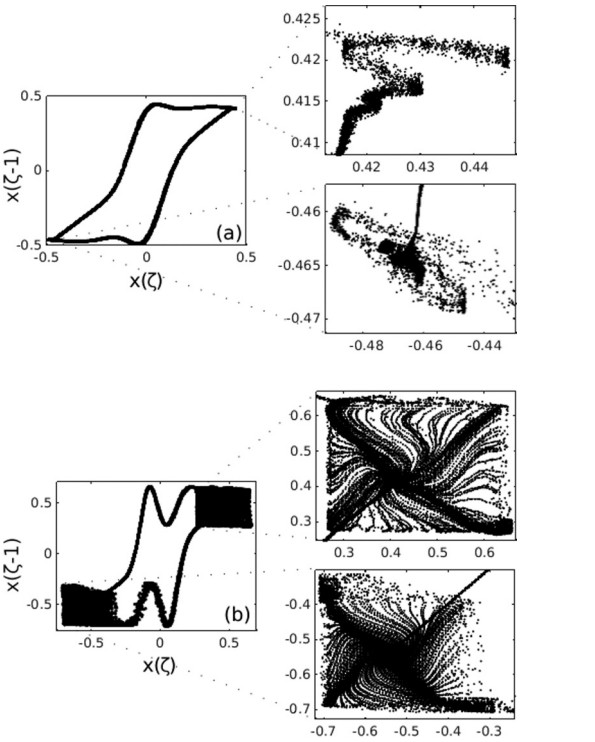

FIG. 6. First-return maps from the time series: (a) $\beta = 1.7$ with the corresponding zoom at the top and bottom extrema, (b) $\beta = 2.2$ with the corresponding zoom at the top and bottom extrema, where $\phi_0 = -\pi/4$.

We have further shown that beyond the Liénard limit-cycle solution, the Liénard-Ikeda solution can be interpreted as the unidirectional coupling of a conventional (i.e., low pass instead of bandpass) Ikeda dynamics and a Liénard limit cycle modulating the phase parameter of the Ikeda dynamics. Our result is demonstrated experimentally by constructing an Ikeda dynamics nonautonomously driven by the typical waveform—a triangular one—typically issued from a Liénard system. Experimental and numerical results are found in excellent agreement, and the results are supported by analytics developed on the original bandpass Ikeda model. As illustrated

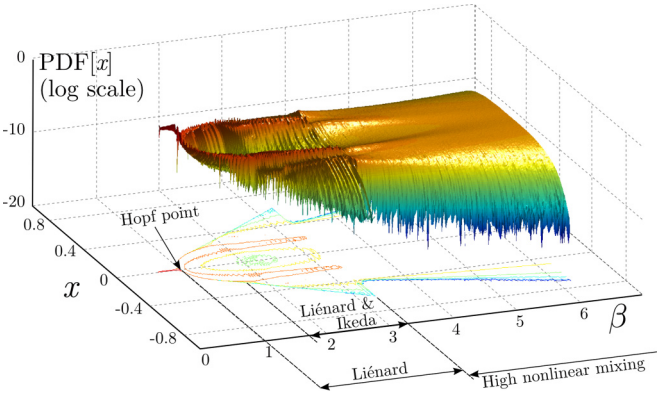

FIG. 7. Numerical simulations of distributions of the orbits $x(t)$ for different feedback gain values β and $\phi_0 = -\pi/4$.

in Fig. 7, when β is further increased (ca. above 3.3), stronger time scales interplay results in the vanishing of the Liénard slow limit cycle and gives rise to fully developed chaos. We anticipate that such fully developed chaos consists of a more complex and probably bidirectional time-scale nonlinear mixing, as clearly shown by the nicely smoothed probability density function profile after the vanishing of the Liénard envelope (see Fig. 7). Future work will focus on the exploration of such system dynamics for strong β, when the three timescales θ, τ, and τ_D are suspected to mutually trigger the chaotic oscillations, thereby inducing a higher complexity in the timescale interactions.

ACKNOWLEDGMENTS

The authors acknowledge the support of the Region Bourgogne Franche-Comté. This work has been performed in cooperation with Labex ACTION program (Contract No. ANR-11-LABX-0001-01). It has also been supported by the ANR project BiPhoProc from the OH-Risque call (Grant No. ANR-14-OHRI-0002-02).

[1] E. N. Lorenz, J. Atmos. Sci. **20**, 130 (1963).
[2] P. Holmes, Phil. Trans. R. Soc. A **292**, 419 (1979).
[3] E. Rössler, Phys. Lett. **57A**, 397 (1976).
[4] M. C. Mackey and L. Glass, Science **197**, 287 (1977).
[5] L. Wang and X. Yang, Electron. Lett. **42**, 1439 (2006).
[6] J. C. Sprott, Phys. Lett. A **366**, 397 (2007).
[7] M. E. Yalcin, Chaos, Solitons Fractals **34**, 1659 (2007).
[8] M. C. Soriano, J. Garcia-Ojalvo, C. R. Mirasso, and I. Fischer, Rev. Mod. Phys. **85**, 421 (2013).
[9] K. Ikeda, Opt. Commun. **30**, 257 (1979).
[10] K. Ikeda, H. Daido, and O. Akimoto, Phys. Rev. Lett. **45**, 709 (1980).
[11] A. Neyer and E. Voges, IEEE J. Quantum Electron. **QE-18**, 2009 (1982).
[12] L. Larger, P.-A. Lacourt, S. Poinsot, and M. Hanna, Phys. Rev. Lett. **95**, 043903 (2005).
[13] Y. C. Kouomou, P. Colet, L. Larger, and N. Gastaud, Phys. Rev. Lett. **95**, 203903 (2005).
[14] K. E. Callan, L. Illing, Z. Gao, D. J. Gauthier, and E. Scholl, Phys. Rev. Lett. **104**, 113901 (2010).
[15] A. Argyris, D. Syvridis, L. Larger, V. Annovazzi-Lodi, P. Colet, I. Fischer, J. Garcia-Ojalvo, C. R. Mirasso, L. Pesquera, and K. A. Shore, Nature **438**, 343 (2005).
[16] L. Larger, Phil. Trans. Roy. Soc. A **371**, 20120464 (2013).
[17] X. S. Yao and L. Maleki, Electron. Lett. **30**, 1525 (1994).
[18] Y. K. Chembo, K. Volyanskiy, L. Larger, E. Rubiola, and P. Colet, IEEE J. Quantum Electron. **45**, 178 (2009).
[19] L. Maleki, Nature Photon. **5**, 728 (2011).
[20] X. Fang, B. Wetzel, J.-M. Merolla, J. M. Dudley, L. Larger, C. Guyeux, and J. M. Bahi, IEEE Trans. Circuits Syst. I, Reg. Papers **61**, 888 (2014).
[21] A. B. Cohen, B. Ravoori, T. E. Murphy, and R. Roy, Phys. Rev. Lett. **101**, 154102 (2008).
[22] T. E. Murphy *et al.*, Phil. Trans. R. Soc. A **368**, 343 (2010).
[23] B. Ravoori, A. B. Cohen, J. Sun, A. E. Motter, T. E. Murphy, and R. Roy, Phys. Rev. Lett. **107**, 034102 (2011).
[24] L. Illing, G. Hoth, L. Shareshian, and C. May, Phys. Rev. E **83**, 026107 (2011).
[25] L. Appeltant, M. C. Soriano, G. V. der Sande, J. Danckaert, S. Massar, J. Dambre, B. Schrauwen, C. R. Mirasso, and I. Fischer, Nat. Commun. **2**, 468 (2011).
[26] L. Larger, M. C. Soriano, D. Brunner, L. Appeltant, J. M. Gutierrez, L. Pesquera, C. R. Mirasso, and I. Fischer, Optics Express **20**, 3241 (2012).
[27] R. Martinenghi, S. Rybalko, M. Jacquot, Y. K. Chembo, and L. Larger, Phys. Rev. Lett. **108**, 244101 (2012).
[28] V. Udaltsov, L. Larger, J.-P. Goedgebuer, M. W. Lee, E. Genin, and W. Rhodes, IEEE Trans. Circ. Syst. **49**, 1006 (2002).
[29] M. Peil, M. Jacquot, Y. K. Chembo, L. Larger, and T. Erneux, Phys. Rev. E **79**, 026208 (2009).
[30] L. Weicker, T. Erneux, O. D'Huys, J. Danckaert, M. Jacquot, Y. Chembo, and L. Larger, Phil. Trans. R. Soc. A **371**, 20120459 (2013).
[31] G. R. G. Chengui, A. F. Talla, J. H. T. Mbe, A. Coillet, K. Saleh, L. Larger, P. Woafo, and Y. K. Chembo, J. Opt. Soc. Am. B **31**, 2310 (2014).
[32] J. H. T. Mbé, A. F. Talla, G. R. G. Chengui, A. Coillet, L. Larger, P. Woafo, and Y. K. Chembo, Phys. Rev. E **91**, 012902 (2015).
[33] T. Matsumoto, L. O. Chua, and M. Komuro, Int. J. Circuit Theory Appl. **14**, 117 (1986).
[34] E. Ott, *Chaos in Dynamical Systems* (Cambridge University Press, Cambridge, 2002).
[35] W. K. S. Tang, G. Q. Zhong, G. Chen, and K. F. Man, IEEE Trans. Circuits Syst. Fundam. Theory Appl. **48**, 1369 (2001).
[36] M. E. Yalcin and S. Ozoguz, Chaos **17**, 033112 (2007).
[37] B. A. Márquez, J. J. Suárez-Vargas, and J. A. Ramírez, Chaos **24**, 033123 (2014).
[38] J. D. Meiss, *Differential Dynamical Systems* (SIAM, Philadelphia, 2007).